# Selection of Burn-Resistant Materials for Oxygen-Driven Turbopumps

Len Schoenman*
*Aerojet TechSystems Company, Sacramento, California*

**NASA goals for reusable space-based, high-performance orbit transfer vehicle (OTV) propulsion systems have resulted in a need for oxygen/hydrogen engines, which include lightweight, highly reliable, liquid oxygen pumps. The selection of ignition- and burn-resistant materials is a major factor in the design of a compact 75,000-rpm turbopump, which can deliver 6 lb/s of liquid oxygen at 5000 psia. The potential operational hazards of rubbing friction and the impact of foreign particles at high velocity were investigated experimentally for a wide range of candidate materials, i.e., nickel, copper, monel, 316 Stainless Steel, Hastelloy-X, Invar-36, and silicon carbide. Test parameters included oxygen pressure and temperature up to 5000 psia and 800°F, respectively. The effect of increasing the $O_2$ pressure from 1000 to 5000 psi is discussed. The applicability of the candidate materials to oxygen pump design was ranked by comparing the experimental results with themselves and an analytically determined parameter, i.e., the burn factor. Nickel and copper demonstrated superior resistance to ignition and burn in the friction rubbing and particle impact tests relative to monel, stainless steel, and nickel-iron base superalloys.**

## Nomenclature

| | |
|---|---|
| $B_f$ | = burn factor, Kcal-s/100 g metal-cm$^2$ |
| $GH_2$,$GO_2$ | = gaseous hydrogen and oxygen, respectively |
| FRT | = friction rubbing tests |
| $H_f$ | = heat of oxidation, Kcal/100 g metal |
| $LH_2$, LOX | = liquid hydrogen and oxygen, respectively |
| $M$ | = particle size, $\mu$m |
| PIT | = particle impact tests |
| $\alpha$ | = thermal diffusivity, cm$^2$/s |

## Introduction

IN a continuing effort to develop a more economical space transportation system (STS), NASA has defined[1] a series of propulsion goals for a new generation of space-based Orbit Transfer Vehicles (OTV). The propulsion system for these vehicles would utilize hydrogen and oxygen as propellants and deliver a specific impulse approaching 500 lb-s/1b. The OTV's would be transported to one of several space stations in the STS Orbiter starting in the mid-1990s. Operating out of a fueling station located near the space station, each of these OTV's will make up to 100 round-trip flights, transporting numerous types of manned and unmanned payloads to and from higher orbits.

The desired performance goals can be approached by utilizing engines that combine higher operating pressures and higher expansion ratio nozzles. The need for longer life and a minimum maintenance design in conjunction with higher operating pressures is the real technical challenge.

## Problem Definition

The industry standard design approach, utilizing fuel or fuel-rich combustion gas to drive a LOX pump, is shown schematically in Fig. 1.

Presented as Paper 84-1287 at the AIAA/ASME/SAE 20th Joint Propulsion Conference, Cincinnati, OH, June 11-13, 1984; received July 3, 1984; revision received Oct. 9, 1984. 

*Research Scientist. Associate Fellow AIAA.

A detailed review of pump-fed bipropellant engine designs has identified three critical areas of engine maintenance common to all designs, i.e., 1) the high-speed (50,000 to 100,000 rpm) dynamic shaft seal which separates the fuel-driven turbine (direct drive or in a fuel-cooled gearbox) from the oxygen pump, 2) excessive wear rates on propellant-cooled rolling contact bearings, and 3) turbine blade wear and cracking resulting from rapid engine transient heating and high operating temperature.

The hazards and life limitations of seals are as follows: High rubbing speeds, when combined with even a minor level of vibration and repeated thermal cycling, result in seal wear and eventual leakage. The potential of hydrogen and oxygen leakage into a common cavity provides an unacceptable explosion hazard.

Existing engine designs, such as the Titan, avoid the interpropellant problem by utilizing an oil lubricated gear system. This, however, results in other maintenance and cooling needs. The RL-10 utilizes $H_2$ propellant cooled gears to synchronize the hydrogen and oxygen pumps and has similar interpropellant seal limitations.

The Space Shuttle Main Engine (SSME) utilizes redundant seals and a helium purge, as shown in Fig. 2. This solution is acceptable, except for the additional weight of the helium purge system. Since ground checks and maintenance are possible following each flight (one engine start per flight), seals with excessive wear and leakage can be replaced. Such is not the case for a space-based OTV where five or more engine restarts may be required for a single mission, and between-flight maintenance is even more costly and difficult.

The technology being developed for the new Aerojet OTV under NASA Contract NAS 3-23772 employs a design concept which eliminates the need for purging and leak-free, high-speed seals. The design shown in Figs. 3 and 4 uses $GO_2$ to drive the LOX pump and $GH_2$ to drive the $LH_2$ pump, thus allowing the drive and pumped fluid to commingle without hazard or loss in performance. Leakage past noncontacting labyrinth seals is recycled internal to the respective pumps which can be all-welded assemblies.

The new pump design eliminates rolling contact bearings which can become a hazard as the bearings age. These are replaced with hydrostatic bearings that will provide unlimited wear life capability.

The engine cycle which makes the $GO_2$ available to drive the turbine does not require high turbine inlet temperatures (400°F) at maximum power and therefore eliminates the usual turbine hot-section life problems.

This new approach, however, is not without concerns relative to the use of high-pressure, high-velocity oxygen. The hazards of metal ignition and burning are the subject of this investigation. The materials ignition hazards associated with the use of warm $GO_2$ in rotating machinery are 1) mechanical rub: thermal growth in bearings and turbine tip, bearing failures, and startup and shutdown transients; and 2) debris: impact of foreign materials and rubbing of foreign materials.

From previously documented experience, it is quite apparent that, along with design, proper material selection is a key factor in demonstrating the concept feasibility. To address these concerns, an analytical and experimental program was instituted to assess the hazard of materials ignition in an oxygen-driven turbine. Tests of friction rubbing and particle impact were performed.

## Test Material Selection

There were two main objectives in the material selection for the experimental program. The first was to determine if the proposed analytical methods for ranking burn resistance of metals would be applicable to the selection of materials for bearings and turbines where rubbing friction and foreign particle impact were possible. The second was to obtain first-hand test experience for the candidate pump, bearings, and turbine materials at $GO_2$ temperatures and pressures approximating the most adverse operating conditions that would be encountered in engine operation.

The materials selected for testing were based on a literature search summarized in the following section.

## Data Base

Aerojet has been involved with the characterization of metals and metal alloys in high-pressure oxygen as early as 1960. In electrically heated tube tests, Dean and Thompson[2] investigated ignition and burning rates of 19 materials up to their melting point temperature in pressurized $GO_2$ between 50 and 800 psia. These data suggested that many, but not all, materials were more susceptible to ignition as the pressure increased and that, once ignited, experienced higher burning rates. This early work identified the most common iron-based alloys and stainless steels to be much more prone to ignition and rapid burning than the nickel-based alloys. Pure nickel appeared to provide exceptional ignition resistance. These tests, however, did not simulate the dynamic environments of high-speed turbines, pumps, bearings, and seals.

A concern exists that static tests comprised of specimens heated in $GO_2$ at elevated pressure do not always reveal the true ignition hazards. The logic maintains that certain materials tend to develop protective oxide scales which resist burning and allow the substrate to become superheated far above the normal ignition temperature. Loss of the scale due to a minor rub or impact of even the smallest foreign particle would result in exposure of fresh metal and an immediate ignition and catastrophic failure. Mechanical impact could also produce additional local heating. More recently, Bates et al.[3] conducted extensive testing involving the rupture of electrically heated rods of various materials in high-velocity, high-pressure, heated oxygen. Their results for a typical 300-series stainless steel alloy are summarized in Fig. 5. For the purpose of comparison, this figure also gives the results obtained by Dean and Thompson.[2] The rupture testing in Ref. 3 demonstrated greater flammability for the 300-series stainless steels than did the earlier heated tube tests. Neither reference provided data in the 5000 psi operating range of the OTV engine.

Bates et al.[3] proposed a simple analytical parameter, defined as the material burn factor, to identify the ignition potential of a material. Most simply stated, the burn factor is the heat of formation of the most stable oxide of the material divided by the material's heat adsorption capability. It is expressed as follows:

$$\mathrm{DBF}_{mp} = [\Delta H^{\circ}_{f(\text{metal oxide})298\ \mathrm{K}} / \Delta H_{298\ \mathrm{K}-\mathrm{MP}} + \Delta H_{\text{fusion(MP)}}]$$

where $H_f$ is the heat of formation of the oxide, $H_{298-\mathrm{MP}}$ is the specific heat of the metal between its fusion temperature and the melting point, and $H_{\text{fusion}}$ is the heat required to melt the metal.

Subsequent work by Gluzek et al.[4] defined a modified burn factor expressed as

$$B_F = \frac{H_f}{\alpha} = \frac{\text{heat of oxidation}}{\text{thermal diffusivity}}$$

Comparison of the metals ranking, using the different burn factor calculations, showed reasonable overall agreement, as indicated in Table 1. Notable exceptions are the relative position of aluminum and nickel.

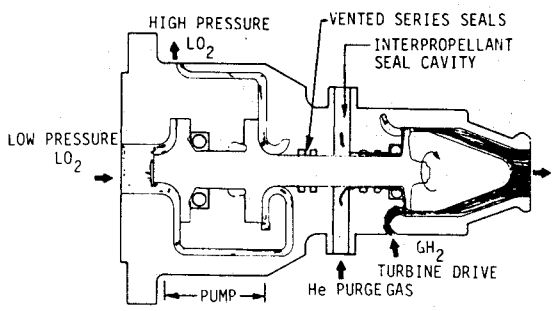


**Fig. 1 Schematic of standard design approach to fuel-rich gas-driven liquid oxygen pumps.**

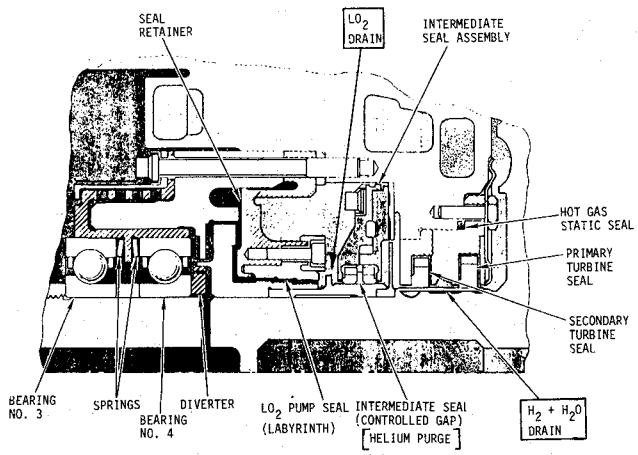


**Fig. 2 Schematic of Space Shuttle Main Engine high-pressure oxygen turbopump bearings and seals.**

**Table 1 Burn factor ranking of typical materials**

| | Dynamic burn factor[3] | $\alpha$ Burn factor[4] |
|---|---|---|
| Best | Silver | Silver |
| | Copper | Copper |
| | Monel 400 | Nickel |
| | Monel K-500 | Aluminum |
| | Nickel | Monel 400 |
| | Iron | Iron |
| | 410 SS | K Monel-500 |
| | 304 SS | 410 SS |
| Poorest | Aluminum | 304 SS |

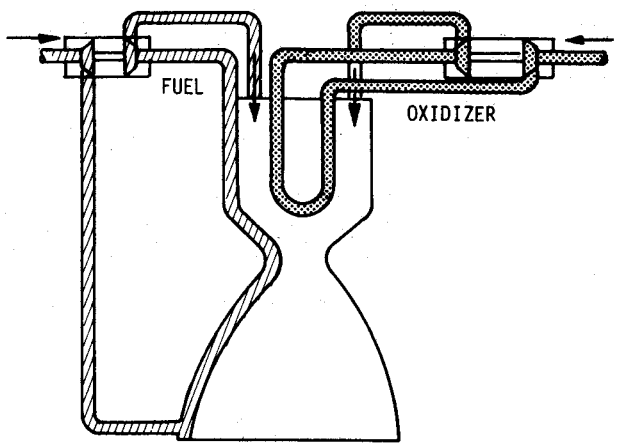


Fig. 3 Schematic of Aerojet dual propellant expander cycle engine.

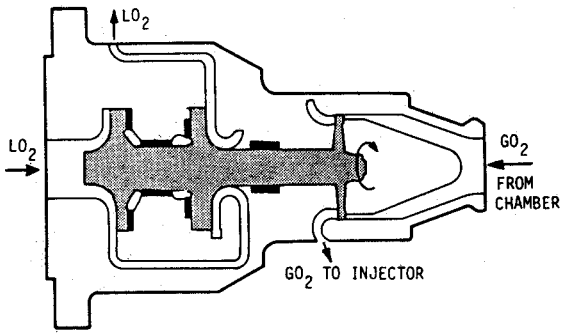


Fig. 4 Schematic of Aerojet design approach to gaseous oxygen-driven liquid oxygen pump for dual-propellant expander cycle engine.

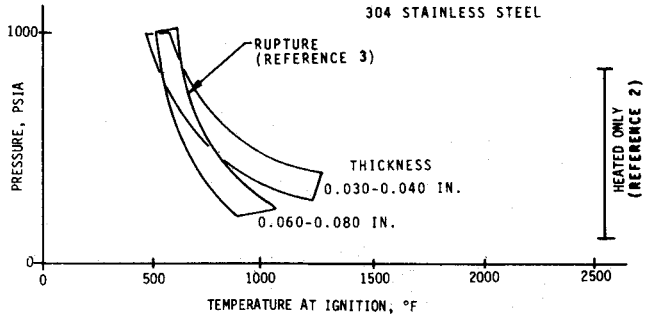


Fig. 5 Comparison of ignition temperatures of stainless steel in heated oxygen gas at high pressure as determined by resistance heating with and without rupture.

The materials for this test program, as shown in Table 2, were selected to provide a wide range of burn factors for candidate turbine and pump materials so that the test results could be correlated with the predictive method. The thermal diffusivity based $B_f$ was selected because it more nearly matched the test results of Ref. 2 in terms of burning rate rank order.

## Test System Description

All testing was conducted at the NASA White Sands Test Facility.

### Friction Rubbing Test (FRT)

The FRT test system, shown in Figs. 6 and 7, consists of a copper-lined cylindrical pressure chamber fabricated from Monel 400 that contains an inner cavity approximately 2 in. in diameter and 2½ in. long. The chamber is provided with a

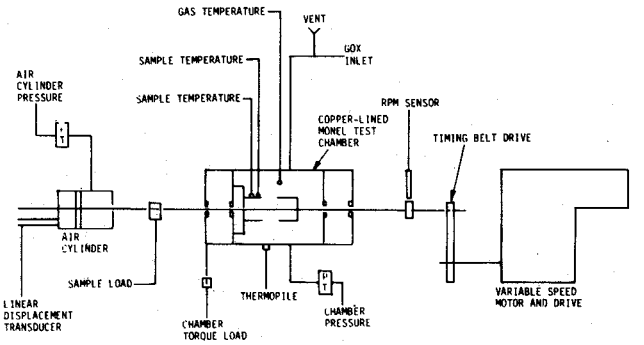


Fig. 6 Schematic of friction rubbing test apparatus.

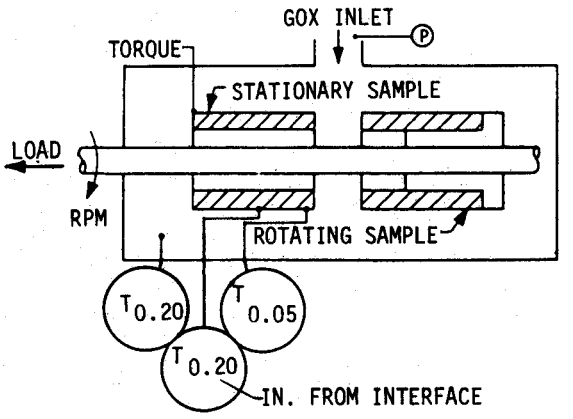


Fig. 7 Schematic of test chamber of friction rubbing test apparatus.

Table 2 Candidate materials tested

| Materials | Burn factor |
|---|---|
| Zr Cu (Cu-150) | 35 |
| Nickel 200 | 550 |
| Silicon carbide | 1145 |
| Monel 400 | 1390 |
| K Monel-500 | 2090 |
| Inconel 600 | 3226 |
| 316 Stainless Steel | 4515 |
| Invar-36 | 5444 |
| Hastelloy-X | 7160 |

rotating shaft that extends through the chamber via a series of water-cooled bearings and seals. The rotating shaft is connected at one end to a drive motor/transmission assembly which is capable of rotating the shaft up to 17,000 rpm. The other end of the shaft is connected to an air actuator which allows axial movement of the shaft and provides the capability of applying up to 1000 lb load on the test sample. Two cylindrical, 1-in.-diam test samples are placed in the chamber. One is mounted to the rotating shaft and the other is fixed to the chamber. The test samples provide 0.283 in.$^2$ of contacting surface. Test sample speeds of approximately 67 ft/s are attained at the maximum rotating speed of 17,000 rpm. The test gas (oxygen) is introduced through a port on the chamber via a facility gas distribution system, which includes an intensifier capable of pressurizing the chamber up to 10,000 psig.

The test system is instrumented as follows. Pressure in the chamber and pressure to the air actuator are measured using bonded strain gage pressure transducers. The temperature of the $GO_2$ environment and the temperature at two locations on the fixed test sample (see Fig. 7) are measured using 304 stainless steel sheathed Chromel-Alumel thermocouples. The usable temperature measurement range is 0–2200°F. The chamber is provided with a thermopile to detect changes in

heat radiation from the rubbing samples. Interface load and torque are measured with specifically positioned load cells. Axial displacement of the rotating shaft is measured using a linear displacement transducer which provides a measure of sample wear and/or sample consumption during burning. Sample surface speed is determined from an rpm sensor and sample radius.

Tests are conducted by bringing the specimens up to the desired rotational speed without load. A ramped compression load of 20 psi/s at the rubbing interface is achieved by loading the shaft which drives the rotating specimen. The load continues to increase until one of the following events occurs.

1) The specimen ignites, as determined by a rapid drop in $O_2$ pressure and increase in specimen temperature.

2) The maximum applied load of 1000 lb is reached.

3) The ram moves its full travel length, 0.2 in., because the specimen has failed in compression or melted.

Figures 8–13 show a typical set of data from a single test.

**Particle Impact Test (PIT)**

The PIT test system consists of a 2-in.-diam (o.d.), 3½-in.-long stainless steel chamber, see Fig. 14, connected to a high-flow, high-pressure, high-temperature $GO_2$ supply. The chamber contains an inner cylindrical cavity which is ¾ in. in diameter and 1 in. long. An orifice assembly is placed at the upstream end of the cylindrical cavity and a target impact plate (test sample) is placed at the downstream side. Three gas exit ports are located symmetrically around the cavity. The orifice assembly and exit restrictions are used to set the $GO_2$ flow rate and/or velocity into the cavity. The target plate and the cup-like backup support fixture are made of the sample material and are positioned perpendicular to the gas flow, as shown in Fig. 14. The thickness of the disk depends on whether the disk is to be ruptured or act as a rigid impact plate when struck by the particles.

The gas supply system consists of storage vessels which contain 500 ft³ of oxygen at 6000 psig. The oxygen supply is controlled by a dome-loaded regulator that maintains essentially

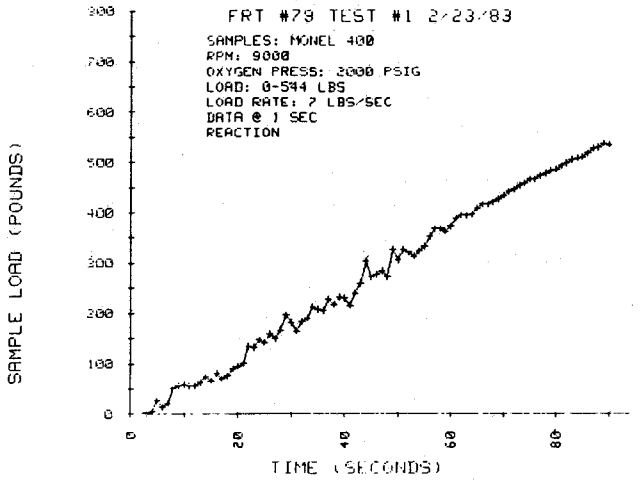


**Fig. 8 Typical data from friction rubbing test, sample load vs time.**

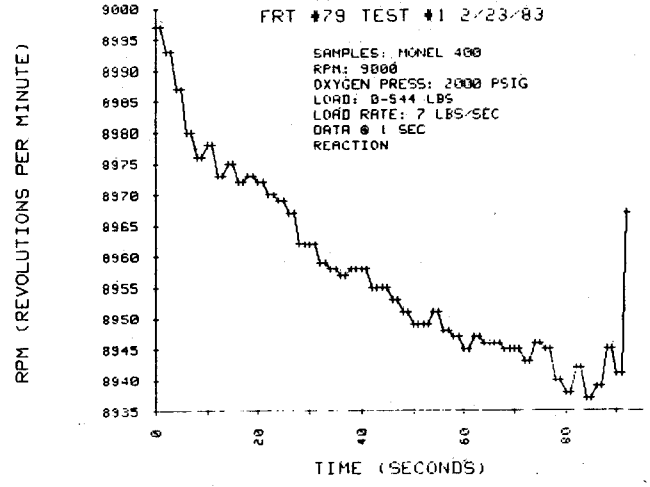


**Fig. 9 Typical data from friction rubbing test, rpm vs time.**

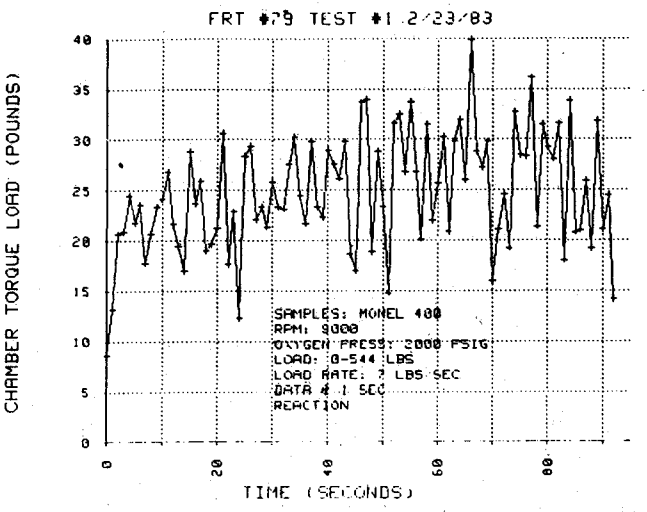


**Fig. 10 Typical data from friction rubbing test, torque load vs time.**

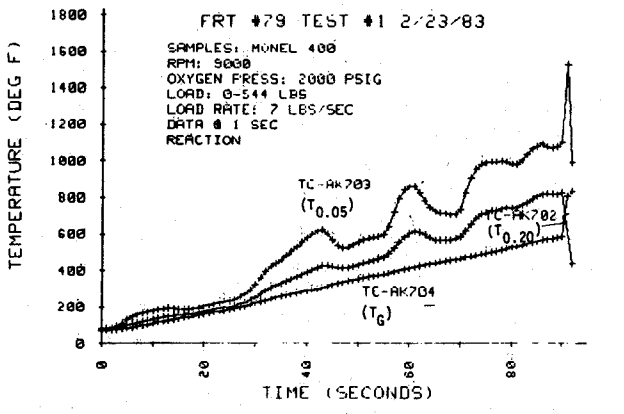


**Fig. 11 Typical data from friction rubbing test, temperature vs time.**

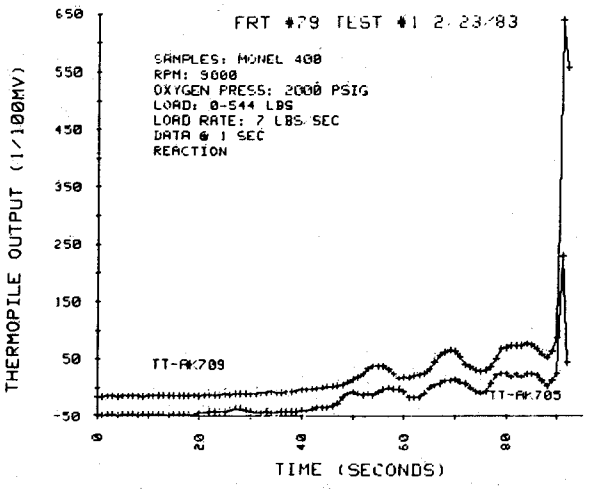


**Fig. 12 Typical data from friction rubbing test, thermopile vs time.**

constant pressure under the flow conditions. A natural gas-fired heat exchanger is located downstream of the dome-loaded regulator and is capable of heating oxygen up to approximately 800°F for 180-s flow periods at 3 lbm/s. The particle injector system is located downstream of the heat exchanger and uses the pressure difference between the flowing oxygen and the injector to insert the test particles into the gas stream.

The test system is instrumented in the following manner. Inlet chamber and cavity gas pressures are measured using bonded strain gage pressure transducers. The inlet chamber and cavity oxygen temperatures are measured using various types of thermocouples, selected on the basis of test conditions and the particular test environment. The gas stagnation temperature and pressure at the impact point were measured and related to the supply conditions during calibration tests. Individual target test measurements were not made during subsequent tests.

The test procedure involves the preheating of the test specimen for 10 and 30 s with $GO_2$, followed by sequential injection of 10 particles of aluminum of 1500 $\mu$m diam. Temperature data from the calibration run established the preheat time. The calibration measurements revealed a standing shock wave ahead of the impact plate. A stagnation pressure of 1700 psia was measured when the pressure upstream of the nozzle reached 4500 psi. The downstream plenum pressure was 500 psia, as illustrated in Fig. 14. Temperatures at the impact plate typically run 40 to 70°F higher than the stream temperatures measured in the upstream flow.

The temperature of the $GO_2$ is increased in each sequential test up to the facility limits of 800°F or until a condition of metal ignition on impact is detected.

A previous test program conducted by Porter[5] at the same facility conducted screening tests of candidate particle materials and sizes. In this earlier program, the materials and particle sizes were selected based on sizes and types anticipated to be found in the Space Shuttle Main Engine propulsion system and led to the selection of 2024 Aluminum and Inconel 718 at the 150 and 800 $\mu$m level. The screening test data showed that aluminum and larger particle sizes provided the greatest probability of ignition up to the temperature limits of the previous test series of 550°F. The present program utilized 1500-$\mu$m aluminum alloy particles propelled by 4500 psi $O_2$ at temperatures up to 800°F.

## Friction Rubbing Test Results

Figure 15 shows a copper-0.15% zirconium alloy test specimen following a 1000 psig, 9000 rpm test. This copper alloy consistently failed in compression as the melting temperature was approached and, in no case, did metal ignition occur.

Table 3 summarizes the 52 tests conducted on similarly configured specimens in 9 materials. In most situations, each test condition was repeated three times and the most adverse results were used for stating ignition threshold.

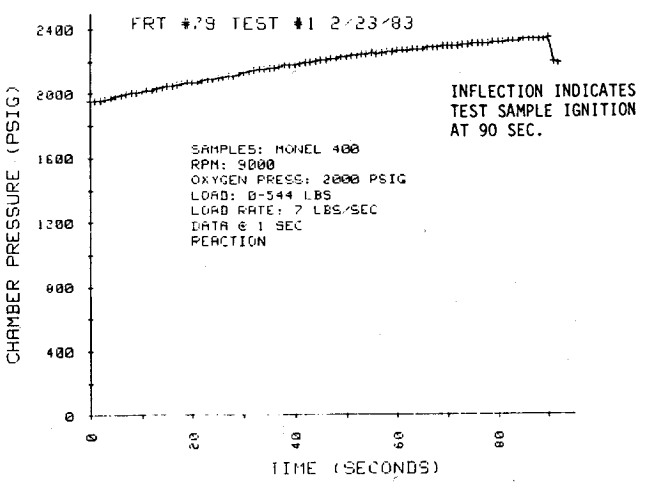


**Fig. 13 Typical data from friction rubbing test, chamber pressure vs time.**

### $O_2$ Pressure Effects

The effect of $O_2$ pressure was evaluated for three materials: Monel 400, 316 Stainless Steel, and Nickel 200, at various rotational speeds.

The results of these tests, shown in Figs. 16–19, were consistent and significantly different from what was expected. The test data indicate that, as the pressures increase above the old data base of 1000 psia, it became progressively more difficult to heat and ignite these materials. Once ignited, the burning at high pressure was more extensive. This, however, may be due to the greater amount of $O_2$ present in the test chamber at the higher pressure.

Figure 16 shows the overlay of the measured temperature 0.05 in. from the contacting surface for Monel 400 at 1000, 2000, and 3000 psi. The time, and thus the work energy, required to heat the specimen to the ignition temperature of 1100°F increased with increasing $GO_2$ pressure. It was not possible to ignite the Monel at 3000 psi, even though the same apparent ignition threshold temperature was reached.

The temperature oscillations observed for the high-pressure test were common throughout the test program and are not fully understood. One possible mechanism could be the buildup of a protective oxide scale which reduces the friction coefficient and the energy generation relative to the conduction cooling. The sharp temperature rise following each drop may be a result of the loss of the oxide scale which exposes fresh metal for oxidation and also increases the frictional heating. The friction coefficient measurements were not sensitive enough in the present apparatus to verify this hypothesis. The equipment, however, is being modified to allow future resolution of this issue.

Figures 17 and 18 compare the time to ignition and load at ignition of 316 Stainless Steel at 19 ft/s surface velocity, and Monel 400 at 35 ft/s as a function of $O_2$ pressure. Note that, at 3000 psi, the Monel 400 did not ignite. The similarity of results in these tests provided encouragement for the view that operation at very high oxygen pressure actually may be less severe than at moderate pressure, and that the more extensive 1000 psi test data base could be effectively utilized for calculating design margins with respect to temperature. Note that similar temperature trends were reported for aluminum, nickel, and copper in Ref. 2.

### Relative Ranking

The relative ranking of materials was accomplished using data obtained at the maximum rpm capability of the machine (17,000 rpm = 67 ft/s) while at 1000 psi oxygen pressure which, at present, appears more adverse than higher pressures. The

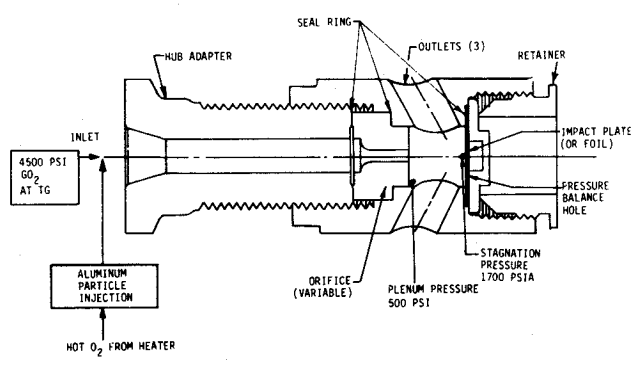


**Fig. 14 Schematic of particle impact test apparatus.**

data shown in Fig. 20 compare the contact pressure attained at the time of ignition for the ramped loading of the three test specimens of each material. The three data points identify the consistency of the test method.

The limitations of the test apparatus, in conjunction with the widely varying compressive strength of the many test specimen materials, resulted in variance in the load application rates from the nominal 20 psi/s.

The load ramp rate values shown in the figure are the mean for the test. Extrusion of the rubbing surface, as shown for copper in Fig. 15, combined with the travel rate limits of the load-applying cylinder, resulted in lower applied load rates for materials experiencing greater displacements at the friction interface.

The most favorable, i.e., burn resistant, materials in Fig. 20 lie to the upper right, while the least favorable are at the lower left, as measured by the total energy imparted to the test specimen.

Comparison of the data with the burn factor ($B_{f\alpha}$) based on room temperature thermal diffusivity is shown in Figs. 21 and 22. Temperature and contact loads at ignition are used as correlating parameters. The data indicate the burn factor does provide a reasonable analytical method for ranking the materials employed in the friction rubbing test.

The line drawn below data in the $B_f$ vs temperature plot contains design margin, in that the temperature shown is measured 0.05 in. from the heated interface. The actual contacting surface could be up to several hundred degrees hotter for the low thermal conductivity materials.

Figure 23 provides a slight refinement of test data in that the burn factor was recomputed using the thermal conductivity at the measured ignition temperature rather than room temperature. The single data point for Monel 400 (M4) is of questionable accuracy and location as there was a temperature measurement problem in that series of three tests.

## Particle Impact Test Results

In this series, each material was tested a minimum of 10 times using 10 particles per test. More extensive testing was

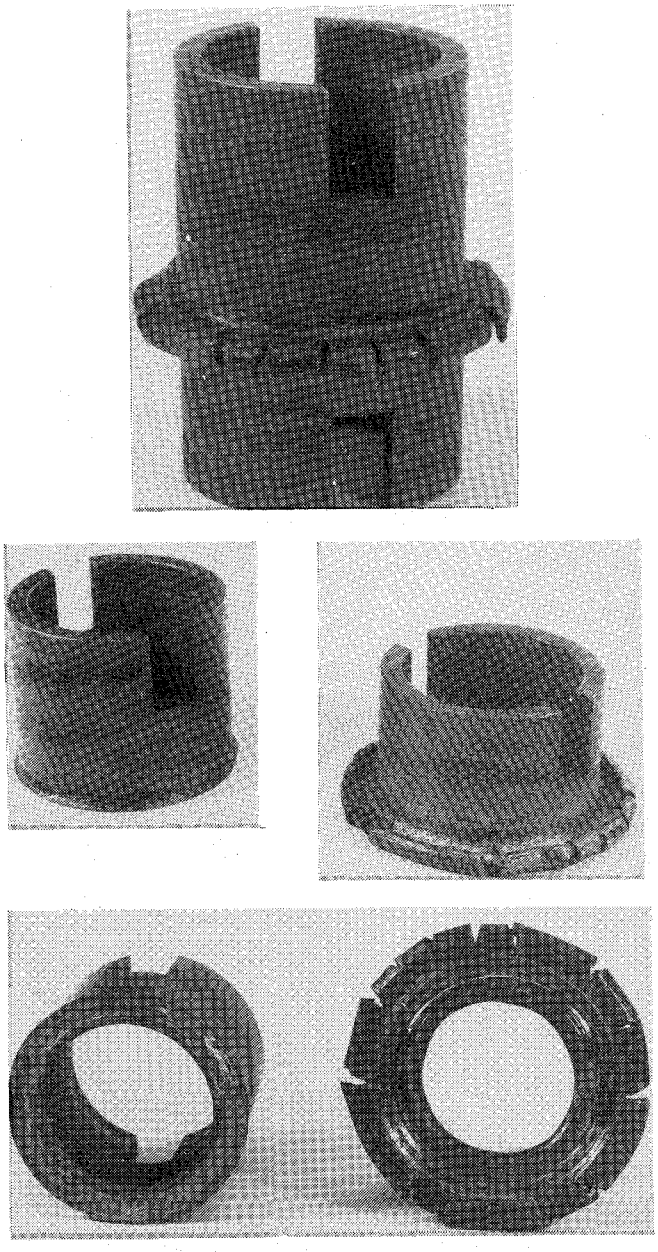

Fig. 15 Copper fails mechanically without igniting [Cu 0.15% Zr specimen (FRT No. 111 1000 psig, 9000 rpm)].

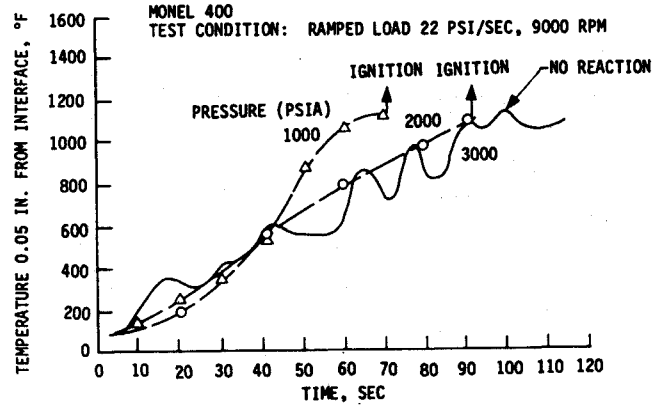


Fig. 16 Effect of $O_2$ pressure on heating rates in friction rubbing tests.

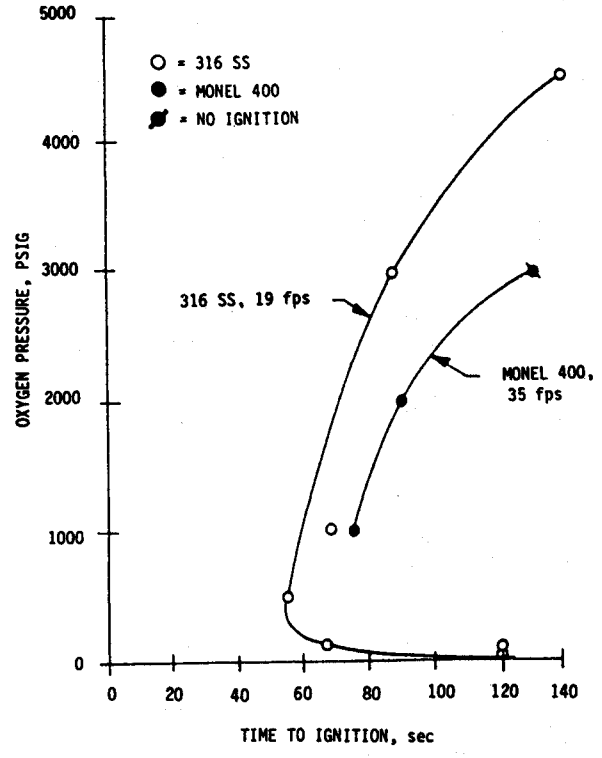


Fig. 17 Test results indicate lower probability of metal ignition in $O_2$ at higher pressure; ignition time.

**Table 3 Test data compilation for friction rubbing tests**

| FRT no. | Speed RPM | Speed ft/s | Pressure, psig | Load,[a] psi | Rate, psi/s | Post-test samples[b] Rotary | Post-test samples[b] Stationary | Time of test/s | Temp °F at 0.05 in. |
|---|---|---|---|---|---|---|---|---|---|
| 316 Stainless Steel | | | | | | | | | |
| 22 | 5000 | 19 | 1000 | 1577 | 16 | R9 | R7 | 100 | 1500 |
| 23 | 5000 | 19 | 1000 | 1450 | 20 | R9 | R7U | 70 | 1400 |
| 24 | 5000 | 19 | 1000 | 1510 | 21 | R9 | R7U | 69 | — |
| 32 | 9000 | 35 | 1000 | 608 | 21 | R6E | R6E | 27 | — |
| 34 | 5000 | 19 | 3000 | 2143 | 24 | R9 | R9 | 86 | 2000 |
| 35 | 3000 | 11 | 1000 | 2705 | 17 | N2 | N2 | >155 | — |
| 84 | 9000 | 35 | 1000 | 597 | 21.3 | R6E | R6E | 28 | 1200 |
| 85 | 9000 | 35 | 1000 | 633 | 18.6 | R6E | R6E | 34 | 1200 |
| 101 | 5000 | 19 | 100 | 1163 | 18.8 | R6E | R6E | 62 | 1600 |
| 102 | 5000 | 19 | 0 | 1984 | 16.5 | N2 | N2 | >120 | >2000 |
| 103 | 5000 | 19 | 50 | 877 | 19 | N2 | N3 | 45 | — |
| 104 | 5000 | 19 | 100 | 1365 | 20.4 | R6E | R6E | 67 | 2200 |
| 109 | 5000 | 19 | 500 | 1234 | | R6E | R6U | 56 | 1800 |
| 140 | 17000 | 67 | 1000 | 406 | 16 | R6E | R6E | 24 | 800 |
| 141 | 17000 | 67 | 1000 | 512 | 18 | N2 | N2 | 28 | 400 |
| 143 | 17000 | 67 | 1000 | 459 | 18 | R6E | R6E | 25 | 1247 |
| | 5000 | 19 | 4500 | 2739 | 19 | | | 138 | .450 |
| Zirconium copper (Cu 150) | | | | | | | | | |
| 111 | 9000 | 35 | 1000 | 1181 | 19 | — | — | | |
| 145 | 17000 | 67 | 1000 | 1043 | 19 | N5 | N2 | | |
| 146 | 17000 | 67 | 1000 | 1209 | 19 | N5 | N2 | 63 | 1650 |
| 147 | 17000 | 67 | 1000 | 1556 | 19 | N2 | N3 | 75 | 1880 |
| 148 | 17000 | 67 | 1000 | 2288 | 15 | N2 | N3 | 115 | 1880 |
| Nickel 200 | | | | | | | | | |
| 142 | 17000 | 67 | 1000 | 1651 | 21 | R7E | R73 | 80 | >2200[c] |
| 144 | 17000 | 67 | 1000 | 2182 | 19 | R8U | R7E | 120 | >2200[c] |
| 156 | 9000 | 35 | 1000 | 2313 | 21 | N3 | N3 | 105 | >2200[c] |
| 157 | 13000 | 51 | 1000 | 2408 | 21 | N3 | N3 | 120 | >2200[c] |
| 158 | 15000 | 59 | 1000 | 2355 | | N3 | N3 | 112 | >2200 |
| 161 | 17000 | 67 | 1000 | 2436 | 22 | N | N | 120 | >2200[c] |
| | 17000 | 67 | 4000 | 2511 | 535[c] | N | N | 25 | >1940 |
| Inconel 600 | | | | | | | | | |
| 195 | 17132 | 67 | 1072 | 1400 | 21.9 | R | R | 64 | 1351 |
| 194 | 17104 | 67 | 1239 | 1950 | 20.1 | R | R | 97 | 1486 |
| 196 | 17094 | 67 | 1088 | 2050 | 21.8 | R | R | 94 | 1109 |
| Silicon carbide | | | | | | | | | |
| 123 | 9000 | 44 | 1000 | 1167 | 13 | N5 | N5 | | |
| 177 | 17000 | 83 | 1000 | 106 | 21 | N5 | | 7 | |
| 178 | 9000 | 44 | 1000 | 244 | 15 | N5 | N1 | 17 | |
| Monel K-500 | | | | | | | | | |
| 179 | 17000 | 67 | 1000 | 1174 | 25 | R6E | R6E | 46 | 1600 |
| 180 | 17000 | 67 | 1000 | 1025 | 25 | R6E | R6E | 42 | 1500 |
| 181 | 17000 | 67 | 1000 | 1025 | 25 | R6E | R6E | 41 | — |
| Monel 400 | | | | | | | | | |
| 162 | 17000 | 67 | 1000 | 1050 | 23.3 | R6E | R6E | 45 | — |
| 163 | 17000 | 67 | 1000 | 1114 | 24.2 | R6E | R6E | 46 | 1200 |
| 164 | 17000 | 67 | 1000 | 1138 | 24.2 | R6E | R6E | 47 | |
| 82 | 9000 | 35 | 3000 | 2791 | 21.7 | N | N | 130 | 1200 |
| 79 | 9000 | 35 | 2000 | 1922 | 21.5 | R | R | 90 | 1070 |
| 75 | 5000 | 19 | 1000 | 2580 | 19.2 | R | R | 134 | 1500 |
| 68 | 9000 | 35 | 1000 | 1689 | 22.5 | R | R | 75 | 1160 |
| 72 | 7000 | 28 | 1000 | 2664 | 19.7 | R | R | 135 | 1600 |
| Invar-36 | | | | | | | | | |
| 149 | 17000 | 67 | 1000 | 686 | 27 | R7E | R7E | 24 | 364 |
| 150 | 17000 | 67 | 1000 | 703 | 27 | R7E | R7E | 25 | 339 |
| 154 | 17000 | 67 | 1000 | 714 | 25 | R9U | R7E | 26 | 900 |
| Hastalloy-X | | | | | | | | | |
| 151 | 17000 | 67 | 1000 | 661 | 20 | R6E | R6E | 33 | 750 |
| 152 | 17000 | 67 | 1000 | 643 | 22 | R6E | R7E | 28 | 1000 |
| 153 | 17000 | 67 | 1000 | 799 | 19 | R6E | R6E | 41 | 1000 |

[a]The contact load normally is the peak contact load within 0.5 s of the reaction. [b]The post-test sample code is as follows. N1: No-reaction, very little wear; N2: No-reaction, slight wear and deformation; N3: No-reaction, mushroomed; N4: No-reaction, melted and totally deformed; N5: No-reaction, shattered; R6: Reaction, ¼ of sample consumed; R7: Reaction, ½ of sample consumed; R8: Reaction, ¾ of sample consumed; R9: Reaction, total sample consumed; E: Even consumption of the rubbing surface; U: Uneven consumption of the rubbing surface; W: Sample welded but did not react; M: Sample melted but did not react. [c]Rapid ramp rate used to attempt ignition, test, or seal failure caused test termination without ignition.

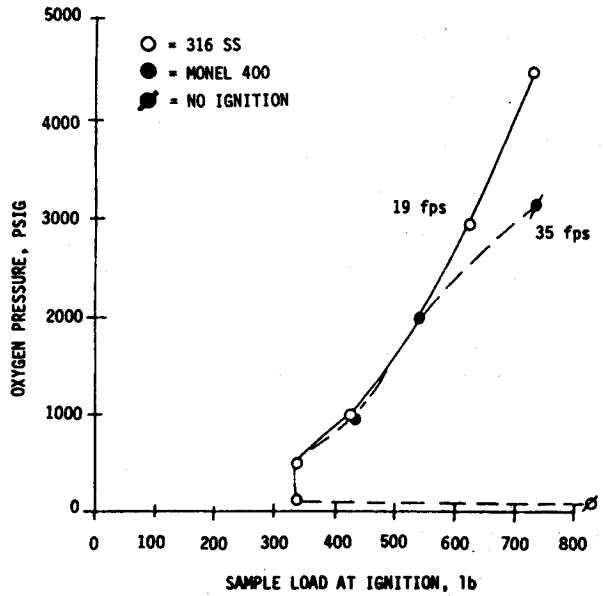


Fig. 18 Test results indicate lower probability of metal/ignition in $O_2$ at higher pressure; sample load.

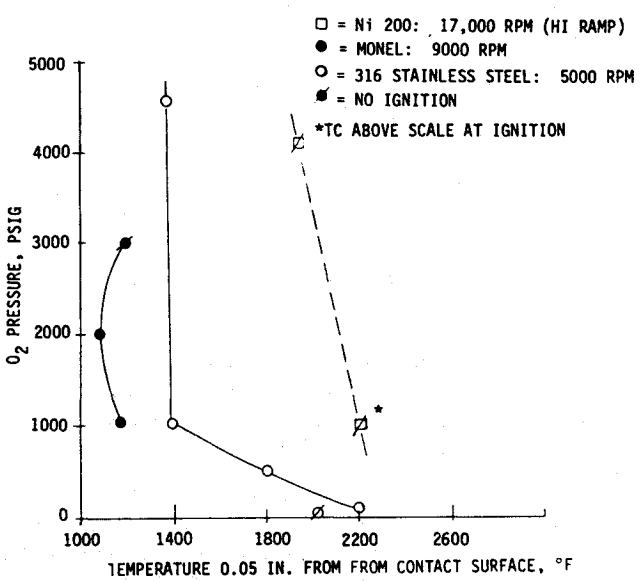


Fig. 19 $O_2$ pressures greater than 1000 psi do not appear to lower ignition temperatures.

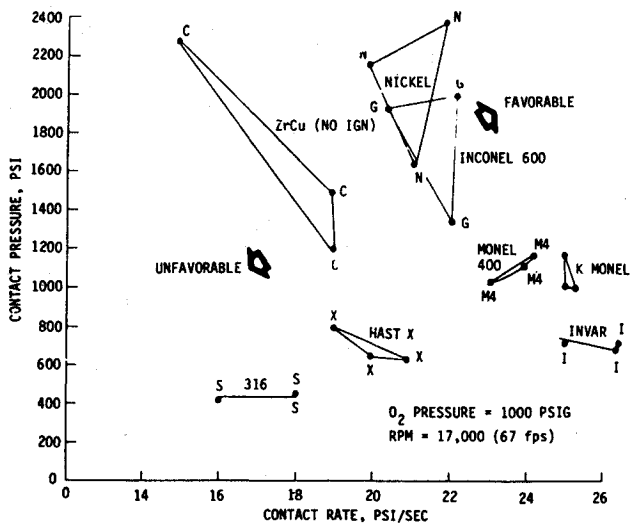


Fig. 20 Relative load limits of selected materials at 1000 psi and maximum speed.

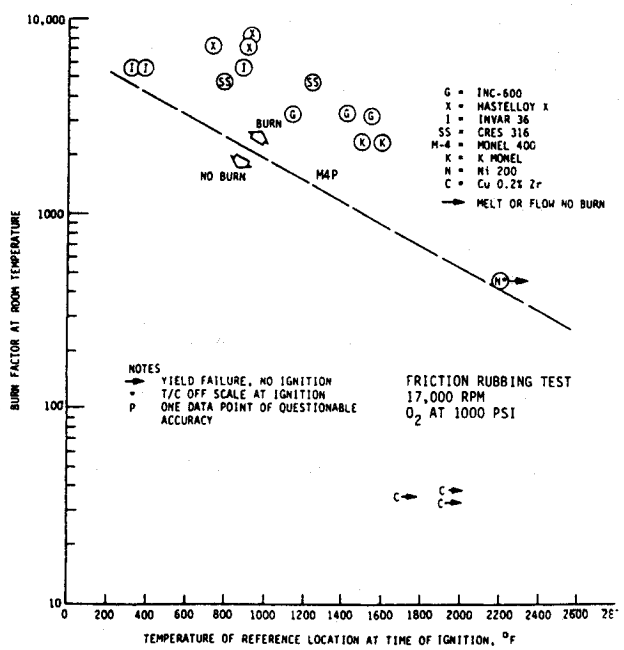


Fig. 21 Burn factor vs ignition temperature in 1000 psi $O_2$.

Table 4 Particle impact test results

| Material | 1500 $\mu$m particle impact at 4500 psi |
|---|---|
| Zirconium copper | o (790°F) |
| Nickel 200 | o (825°F) |
| K Monel-500 | ⊖ (750–825°F) |
| Monel 400 | o (800°F) |
| Silicon carbide | o (750–820°F) Material shatters on impact |
| Hastelloy-X | ● (725°F) |
| Invar-36 | ● (700°F) |
| 316 Stainless Steel | ● (450°F) |

Note: o indicates no ignition occurs up to indicated oxygen temperature, ⊖ surface reaction and quench occurs at indicated oxygen temperature, and o burning occurs at indicated temperature. Temperatures in parentheses are measured upstream of orifice; temperatures at impact plate could be 40 to 70°F higher.

conducted on 316 Stainless Steel and Nickel 200 where material thickness was also varied.

Typical test results for 1500-$\mu$m particles propelled by 4500 psi $GO_2$ on 316 Stainless Steel and Ni 200 foil and plate are displayed in Fig. 24. The test data show rupture of the thin foil produces no greater ignition hazard than the impact of the aluminum particles on the more rigid plate. Subsequent testing on other materials was conducted utilizing the plate.

These tests show that, when the $O_2$ temperature exceeded 420°F, a high $B_f$ material, like 316 Stainless Steel, is ignitible. In contrast, no ignitions were experienced with nickel up to the limits of the test facility capability, even when thin foils (0.005 in.) were ruptured. The thin foils were initially chosen to represent thin leading and trailing edges of small turbine blades. Table 4 itemizes the lowest $GO_2$ temperature that produced an ignition.

**Table 5 Burn factor ranking criterion for materials selection for high-pressure, gaseous oxygen applications**

| Material | Burn factor | Observations |
|---|---|---|
| Zirconium copper | 35 | No ignition in any tests (790/1800°F)[a] |
| Nickel 200 | 550 | Ignition above 2200°F in FRT only (825/2200°F) |
| Silicon carbide | 1145 | No ignition in limited testing (850/ – °F) |
| Monel 400 | 1390 | Ignition above 1200°F FRT only (800/1200°F) |
| K Monel-500 | 2090 | Ignition above 1500°F FRT (750/1500°F) |
| Inconel 600 | 3226 | Ignition above 1100°F (—/1000°F) |
| 316 Stainless Steel | 4515 | Ignition in all tests (450/800°F) |
| Invar-36 | 5444 | Ignition in all tests (675/340°F) |
| Hastelloy-X | 7160 | Ignition in all tests (725/750°F) |

[a]Temperatures from particle impingement test friction rubbing test (FRT) at 1000 psi and 17,000 rpm.

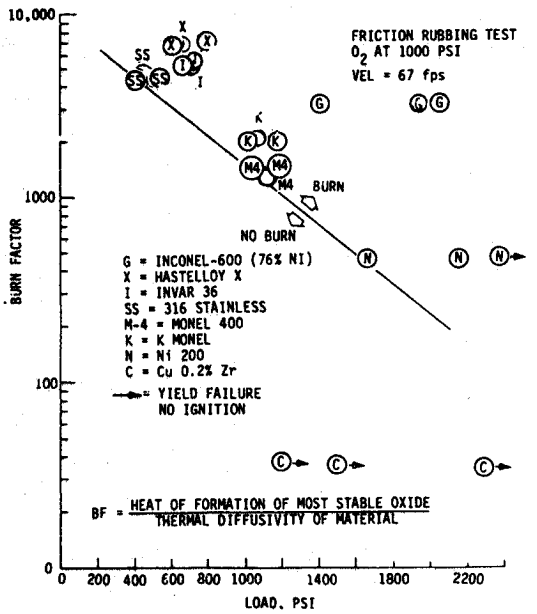


**Fig. 22 Burn factor vs load at ignition in 1000 psi $O_2$.**

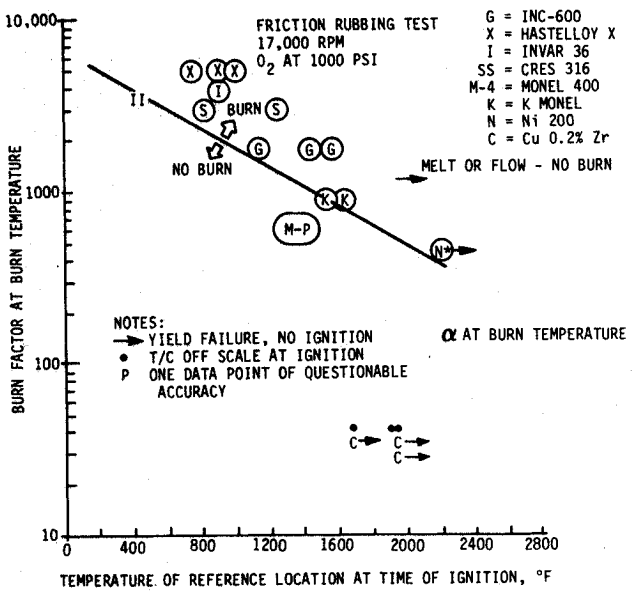


**Fig. 23 Burn factor vs ignition temperature in 1000 psi $O_2$.**

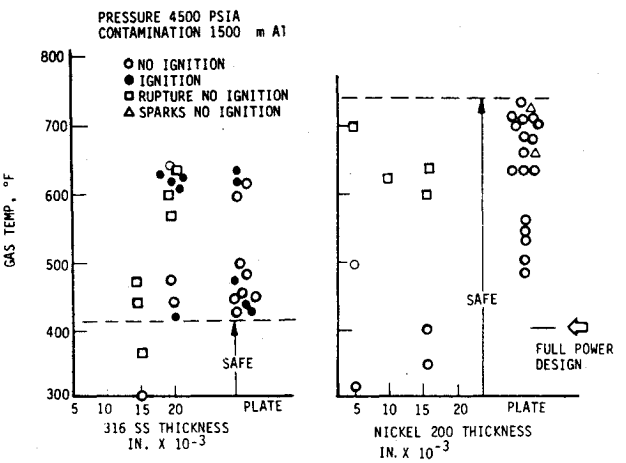


**Fig. 24 Typical particle impact test results.**

## Comparison of Results of Two Test Methods and Conclusions

Table 5 lists the materials in order of increasing burn factor and provides a comparison with observations from the two test methods.

Nickel and copper, which have burn factors under 1000, were the safest materials tested. Copper never experienced an ignition and nickel only ignited above the 2200°F limits of the instrumentation capabilities. The silicon carbide, which tended to shatter at relative low impact loads (mainly because of poor specimen design for the ceramic properties), never ignited in the limited testing conducted. Materials with burn factors equal to Monel and high nickel alloys (1200 to 3000) were ignitible only in the FRT test. Also, materials with high burn factors (above 4000) were easily ignitible at relatively low temperatures by both test methods. The burn factor, therefore, can be concluded to be a valid method of screening candidate metals for potential application in high-pressure $GO_2$ service.

It is apparent that many of the past catastrophic failures in oxygen systems may have developed due to poor design. However, the more likely cause of failure is poor materials selection. Invar, for example, can ignite at temperatures as low as 340°F. This material has often been used to contain low expansion coefficient carbon-based seals in LOX turbopumps. In reflecting on the present data, in relation to past design practices, there is little wonder that machines utilizing high-pressure oxygen cause concern.

In looking to the future, it is the intent of this OTV technology program to pave the way to the safe use of high-pressure $O_2$, not by trial and error failures, but by sound

design practices and a more scientific approach to materials selection.

### Acknowledgments

The author would like to thank the following members of the NASA for coordinating the test program and conducting the test activities: Larry Cooper, NASA Lewis Research Center, and Frank Benz, Joel Stoltzfus, and Randy Shaw, NASA White Sands Test Facility.

### References

[1]Cooper, L.P., "Advanced Propulsion Concepts for Orbital Transfer Vehicles," NASA TM-8-3419, June 1983.

[2]Dean, L.E. and Thompson, W.R., "Ignition Characteristics of Metals and Alloys," *ARS Journal,* July 1961.

[3]Bates, C.E., Wren, J.E., and Pears, C.D., "Ignition and Combustion of Ferrous Metals in High-Pressure, High-Velocity Gaseous Oxygen," *Journal of Material for Energy Systems*, Vol. 1, June 1979, pp. 61–76.

[4]Gluzek, F., Mokadam, R.G., To, I.H., Stanitz, J. D., and Wollschlager, J., "Liquid Oxygen/Liquid Hydrogen Boost Vane Pump for Advanced Orbit Transfer Vehicle Auxiliary Propulsion System," NASA CR-159648, Sept. 1979.

[5]Porter, W.S., "Test Report, Metals Ignition Study in Gaseous Oxygen," NASA/White Sands Test Facility, TR 277-001, Oct. 1982.